

# Simplified Measurement of Deoxyglucose Utilization Rate

George J. Hunter, Leena M. Hamberg, Nathaniel M. Alpert, Noah C. Choi and Alan J. Fischman

Departments of Radiology and Radiation Oncology, Massachusetts General Hospital and Harvard Medical School, Boston, Massachusetts

The reliability of the dose uptake ratio (DUR), a widely used index of  $^{18}\text{F}$ -fluoro-2-deoxy-D-glucose ( $^{18}\text{F}$ FDG) metabolism in a variety of tumors, depends on the overall rate of removal of  $^{18}\text{F}$ FDG from the circulation. Correcting for this factor is important if DUR is to be used quantitatively for pre- and post-treatment assessments of tumors. **Methods:** We developed a simplified kinetic method (SKM), based on measured blood curves from a control group, which requires one venous blood sample. We compared the simplified method to the conventional kinetic method and the widely used DUR index in 13 patients with grade 3 or 4 non-small-cell lung carcinoma. Studies were obtained before and after treatment. In all patients, dynamic PET imaging and blood activity measurement was performed for 80 min. The utilization rate of  $^{18}\text{F}$ FDG (MRDGlc) was calculated by using a three-compartment model and correlated with a 55-min measurement of DUR and with the simplified kinetic method. **Results:** Coefficients of determination ( $R^2$ ) between MRDGlc and DUR before and after treatment were 0.53 and 0.71, respectively. Using the SKM, these values improved significantly ( $p < 0.0001$ ) to 0.96 and 0.94, respectively. The pooled pre- and post-treatment coefficient of determination for DUR versus MRDGlc was 0.81; for SKM, it improved significantly ( $p < 0.001$ ) to 0.98. **Conclusion:** These results indicate that the observed tumor tissue uptake of  $^{18}\text{F}$ FDG, corrected for blood  $^{18}\text{F}$ FDG activity and glucose concentration, can reliably predict glucose metabolic rate from a single static image acquired at between 45 min and 1 hr after injection. This has substantial implications for the quantitative use of  $^{18}\text{F}$ FDG PET to diagnose and manage malignancy.

**Key Words:** fluorine-18-FDG; PET; dose uptake ratio; glucose metabolism; lung cancer; diagnostic imaging

**J Nucl Med 1996; 37:950-955**

The deoxyglucose method was first introduced by Sokoloff and colleagues to make quantitative measurement of local glucose metabolism in the "normal" brain of animals (1). Over the years, the deoxyglucose method has been extended to clinical studies in human subjects with PET. For example, PET with  $^{18}\text{F}$ -fluoro-2-deoxy-D-glucose ( $^{18}\text{F}$ FDG) has been used for the clinical investigation of many types of tumor, including those in the brain (2), lung (3-6), head and neck (7-10), reticuloendothelial system (11-15), musculo-skeletal system (16,17), breast (18-20), bladder (21), pituitary (22,23), colon (24,25), liver (26) and thyroid (27). In general,  $^{18}\text{F}$ FDG PET has proven to be of significant value in prognosis, evaluation of malignant degeneration and determination of recurrence and dissemination of neoplasia after radiation or chemotherapy (24,28-32). However, rigorous application of the deoxyglucose method in clinical investigation is complicated by pathophysiological as well as practical considerations.

Pathophysiological considerations include the possibility that

the relationship between deoxyglucose and native glucose differs in different tissue types, for example, in certain tumors, thus causing the lumped constant to vary. Practical considerations include those related to the length and invasiveness of the examination. Ongoing research, in several centers, has focused on understanding the relationship between the metabolism of glucose and deoxyglucose in different tumor types. Another line of investigation seeks to deal with the practical considerations outlined above through simplifications of the methodology. That is the goal of the present study.

If it is necessary to characterize different tumor types, differentiate therapeutic response from recurrence, compare studies in the same patient obtained at different times or compare studies obtained at different institutions, a precise and reliable method for quantifying the accumulation of  $^{18}\text{F}$ FDG is necessary (33-36). Such a method would serve as a standard with which to assess the diagnosis and treatment of neoplasia. This requirement is fulfilled by quantification of tissue deoxyglucose metabolic rate (MRDGlc) obtained from a detailed tracer kinetic analysis of dynamic  $^{18}\text{F}$ FDG PET data. Unfortunately, in many clinical situations, patients cannot tolerate the prolonged imaging times required for such studies, or arterial blood sampling may not be feasible. Furthermore, many busy clinical PET centers are not always able to devote sufficient time to the acquisition of the data needed to calculate MRDGlc.

To reduce the time required for data acquisition and analysis, while still providing a clinically useful measure of tumor metabolic activity, the semi-quantitative DUR index of  $^{18}\text{F}$ FDG utilization was developed (33,35). Typically, DUR is calculated from a static acquisition obtained between 45 and 60 min after injection; one simply divides the  $^{18}\text{F}$ FDG activity in a tumor region of interest by the injected dose, normalized to the patient's weight. This yields a dimensionless parameter which equals unity if there is uniform, homogenous distribution of  $^{18}\text{F}$ FDG throughout the body. Although measurements of DUR have been extensively used in many clinical examinations, fundamental problems with its application remain, despite many attempts to address them through a variety of correction techniques. For instance, since accumulation of  $^{18}\text{F}$ FDG is low in adipose tissue, DUR may be overestimated in obese patients (37). To address this issue, several investigators have proposed normalizing to lean body weight. Other groups have proposed corrections based on plasma glucose levels (38,39). Neither the original measurement nor any of its derivatives overcome all of the potential errors inherent in DUR. These can be surprisingly large; for example, for lung tumors in which plateau levels of  $^{18}\text{F}$ FDG accumulation have not been achieved at the time of measurement (the usual case with a static acquisition taken at 45-60 min), errors in the DUR fall unpredictably between 20% and 70% pre-treatment, and between 5% and 40% after treatment (40).

The theoretical basis upon which MRDGlc is calculated (1)

Received Mar. 31, 1995; revision accepted Aug. 17, 1995.

For correspondence or reprints contact: Alan J. Fischman, MD, Division of Nuclear Medicine, Department of Radiology, Massachusetts General Hospital, White 2, Fruit St., Boston, MA 02114.

suggested to us an alternative approach that would retain the simplicity of DUR while providing an improved and quantitative measure of tumor metabolism. In this study, we present a simple, single time-point methodology for generating an accurate predictor of tissue glucose metabolic rate. With this technique, the only requirement is a 15 min static image acquired at between 45 and 60 min after injection of  $^{18}\text{F}$ FDG and a timed blood sample collected at  $\sim 55$  min after injection. We validated the method by correlating SKM results with true  $^{18}\text{F}$ FDG metabolic rates derived from the 80-min dynamic data set by full kinetic analysis.

## MATERIALS AND METHODS

### Subjects

Thirteen patients with primary Stage III or IV non-small-cell lung cancer were studied by dynamic and static  $^{18}\text{F}$ FDG PET. The protocol was approved by the human studies committee of Massachusetts General Hospital, and written, informed consent was obtained from each patient. Paired studies were performed in each patient. The first study was performed before treatment, and the second 2 wk after completion of therapy. The patients fasted for at least 8 hr before imaging. Blood glucose concentration was determined immediately before the study.

Tumor location was determined by computed tomography. Tumor grade and type were known from previous biopsy or staging surgery. None of the patients suffered from diabetes mellitus.

### Fluorine-18-FDG Synthesis

Fluorine-18 was prepared by 17 MeV proton bombardment of an  $\text{H}_2^{18}\text{O}$  target (41).  $^{18}\text{F}$ FDG was prepared by robotic implementation of the method of Hamacher et al. (42,43). The radiochemical purity of the product was evaluated by HPLC and TLC and was greater than 98%. Pyrogen testing was performed by using the 30-min limulus test.

### Quantitative FDG-PET Study

All imaging was performed with an 8-ring whole-body imaging system. The primary imaging parameters of this instrument are in-plane and axial resolutions of 6.0 mm FWHM, 15 contiguous slices of 6.5 mm separation and a sensitivity of 5,000 cps/ $\mu\text{Ci}/\text{ml}$  (44). All images were reconstructed using a conventional filtered back-projection algorithm to a final in-plane resolution of 7 mm FWHM. Transmission scans, acquired with a rotating pin source containing  $^{68}\text{Ge}$ , were used to confirm positioning and to correct for tissue attenuation. All projection data were corrected for non-uniformity of detector response, dead time, random coincidences and scattered radiation. The PET camera was cross-calibrated against a well scintillation counter by comparing the camera's response, obtained from a uniform distribution of an  $^{18}\text{F}$  solution in a 20 cm cylindrical phantom, with the response of the well counter to an aliquot of the same solution.

The patients were positioned supine on the imaging bed of the PET scanner with arms extended out of the field of view. Dynamic image collection was started immediately before intravenous injection of approximately 10 mCi of  $^{18}\text{F}$ FDG. Sequential images were acquired in 15-sec frames for the first 1.75 min, 30-sec frames for the next 2 min, 60-sec frames for the next 2 min, 2-min frames for the next 4 min, 5-min frames for the next 20 min, 10-min frames for the next 40 min and a 15-min frame for the final 15 min.

Arterial input curves were measured from arterial blood samples, regions of interest over the left ventricle or regions of interest over the ascending aorta. Several areas of the tumor were chosen for analysis by selecting regions of interest above the 90<sup>th</sup> percentile for  $^{18}\text{F}$ FDG activity in the tumor as visualized in the final acquisition. This strategy was used to exclude necrotic areas from the analysis. The average time-activity curve for all the sampled

regions in each tumor was calculated. Analysis using a three-compartment  $^{18}\text{F}$ FDG kinetic model (1,40,45) yielded the rate constants for  $^{18}\text{F}$ FDG metabolism in metabolically active regions of the tumors. The lumped constant is unknown in this tumor and was taken to be unity.

From the images acquired between 45 and 60 min, a conventional DUR was calculated for each patient by dividing the tumor tissue  $^{18}\text{F}$ FDG activity in the region of interest by the actual injected dose and normalized to body weight. The SKM value of MRDGlC for tumor tissue was calculated by correcting the observed  $^{18}\text{F}$ FDG activity at 55 min with the blood  $^{18}\text{F}$ FDG activity at 55 min and the blood glucose concentration. Coefficients of determination between actual MRDGlC, DUR and SKM values for MRDGlC were calculated.

### Calculation of Glucose Metabolic Rate

Tissue time-activity curves were fitted to a 3-compartment, 3-rate constant model of  $^{18}\text{F}$ FDG transport and metabolism. If it is assumed that the disappearance of  $^{18}\text{F}$ FDG from plasma can be described by a tri-exponential function, integration of the model equations yields the following expression for the time dependence of the concentration of  $^{18}\text{F}$ FDG in tissue:

$$C_T(t) = \frac{K_1 k_2}{k_2 + k_3} e^{-(k_2 + k_3)t} \sum_{i=1}^3 A_i \left[ \frac{1 - e^{-(b_i - (k_2 + k_3))t}}{b_i - (k_2 + k_3)} \right] + \frac{K_1 k_3}{k_2 + k_3} \sum_{i=1}^3 A_i \left[ \frac{1 - e^{-b_i t}}{b_i} \right], \quad \text{Eq. 1}$$

where  $K_1$  and  $k_2$  are the rate constants for  $^{18}\text{F}$ FDG transport from plasma into tissue and from tissue back into plasma, respectively, and  $k_3$  is the rate constant for  $^{18}\text{F}$ FDG phosphorylation.  $k_4$ , the rate constant for  $^{18}\text{F}$ FDG dephosphorylation, was assumed to be zero (40).  $b_1$ ,  $b_2$  and  $b_3$  are the rate constants for the disappearance of  $^{18}\text{F}$ FDG activity from whole blood. For simplicity, Equation 1 may be recast in terms of three parameters:  $P_1$ ,  $P_2$  and  $P_3$ , where

$$P_1 = K_1 \quad P_2 = \frac{K_1 k_3}{k_2 + k_3} \quad P_3 = k_2 + k_3$$

yielding

$$C_T(t) = \left[ (P_1 - P_2) \sum_{i=1}^3 \frac{A_i}{P_3 - b_i} (e^{-b_i t} - e^{-P_3 t}) \right] + P_2 \left\{ \sum_{i=1}^3 \frac{A_i}{b_i} (1 - e^{-b_i t}) \right\}. \quad \text{Eq. 2}$$

The tumor tissue time-activity curves were fitted by using Equation 2 with a nonlinear least-squares technique. From the fitted data,  $K_1$ ,  $k_2$  and  $k_3$  were derived for each study. The glucose metabolic rate, MRDGlC, is calculated from  $P_2$  by multiplying with the blood glucose, i.e.,

$$\text{MRDGlC} = P_2 \times \text{Blood Glucose}. \quad \text{Eq. 3}$$

DUR is calculated from the tissue activity  $C_T(t)$  by normalizing to the injected dose and the patient's weight, i.e.,

$$\text{DUR} = \frac{C_T(t)}{\text{Dose/Weight}}. \quad \text{Eq. 4}$$

By letting  $\alpha$  and  $\beta$  represent the terms in curly and square brackets in Equation 2, and rearranging ( $\beta$  is simply the area under the blood activity curve from 0 to time  $t$ ), the relationship between MRDGlC and tissue activity may be more clearly seen:

**TABLE 1**  
Coefficients of the Tri-exponential Fit to the Blood Activity Curve

	Patient no.	A1	A2	A3	b1 (1/min)	b2 (1/min)	b3 (1/min)
Pre-treatment	1	5151.04	776.33	484.58	16.0549	0.2810	0.0076
	2	3505.86	883.72	793.17	2.8106	0.1956	0.0125
	3	1801.10	462.89	380.04	3.4919	0.2159	0.0102
	4	6516.89	1087.78	757.53	12.0480	0.5024	0.0181
	5	1381.52	840.43	1106.55	19.2712	0.2216	0.0075
	6	6055.40	1134.28	954.83	4.1178	0.1630	0.0093
	7	6329.16	983.11	774.11	7.2448	0.3748	0.0119
	8	15560.97	657.56	424.55	18.6229	0.2836	0.0137
	9	7327.09	709.33	720.74	6.7159	0.1992	0.0103
	10	4010.69	977.72	703.64	10.4955	0.4238	0.0176
	11	3257.40	897.70	791.38	3.1263	0.1884	0.0125
	12	5483.87	971.96	690.44	4.2370	0.1991	0.0076
	Post-treatment	1	4350.34	636.61	455.19	7.6505	0.4942
1		8969.48	1193.64	914.09	8.7960	0.2858	0.0138
2		6470.82	1184.92	1134.43	9.7740	0.3607	0.0163
3		1272.54	680.37	601.66	17.3010	0.3365	0.0104
4		6516.89	1087.78	757.53	12.0480	0.5024	0.0183
5		8601.67	623.01	636.82	6.8921	0.1184	0.0075
6		8205.56	988.14	954.83	6.8921	0.1541	0.0108
7		9557.20	666.64	822.67	9.7090	0.1904	0.0081
8		4000.90	563.79	570.13	6.9168	0.2118	0.0124
9		5627.59	866.42	774.27	8.3634	0.3893	0.0139
10		6344.30	822.88	785.36	12.8727	0.3842	0.0179
11		6197.18	886.29	694.10	10.7514	0.2553	0.0124
12		4993.37	692.53	497.35	5.0706	0.2137	0.0088
13	7041.44	854.31	666.32	11.2335	0.3572	0.0164	
				Mean	9.33/min	0.289/min	0.0125/min
				s.e.m.	0.92/min	0.022/min	0.0007/min
				Half-Life	4.46 sec	2.40 min	55.38 min

A1, A2, A3, b1, b2 and b3 are the coefficients of a tri-exponential fit to the timed arterial blood activity curve represented by:  $y = A1 * \exp(-b1 * t) + A2 * \exp(-b2 * t) + A3 * \exp(-b3 * t)$ . The mean and standard error (s.e.m.) of the rate constants b1, b2 and b3 are shown together with the half-lives of blood activity which they represent.

$$P_2 = \frac{C_T(t) - \alpha}{\beta} \quad \text{Eq. 5}$$

The relative contribution of the  $\alpha$  term is quite small (of the order 10%), and is greatest at early time points and when MRDGlc is low (i.e., following treatment). Omitting this term leads to a systematic error which results in over estimation of MRDGlc at low levels of activity and under estimation of MRDGlc at high levels of activity. This approximation, similar to that used by Rhodes et al. (46), forms the basis of our analysis, yielding:

$$P_2 = \frac{C_T(t)}{\beta} \quad \text{Eq. 6}$$

The relationship of  $P_2$  to DUR can be written as:

$$P_2 \propto \frac{\text{DUR}}{\beta} \quad \text{Eq. 7}$$

This shows that before  $\beta$ , the cumulative integral of the blood curve, reaches its asymptotic value, DUR may be a poor approximation to MRDGlc (40).

The key question is how to estimate the area under the blood time-activity curve without the need for measurements at multiple time points. This may be achieved in the following manner. If the decay constants  $b_1$ ,  $b_2$  and  $b_3$  are known a priori, and if  $A_1$ ,  $A_2$  and  $A_3$  can be determined, then an estimate of the area under the blood curve is possible. We observed that the decay constants generally

varied within quite narrow limits for the non-diabetic patient group that we studied (Table 1). Thus, we were able to substitute mean values for individual values with little loss of accuracy.

The determination of  $A_1$ ,  $A_2$  and  $A_3$  requires further information, specifically, the actual  $^{18}\text{F}$ FDG activity in the blood at a known time, the dose of  $^{18}\text{F}$ FDG injected and the circulating blood volume in each patient. An individual's circulating blood volume may be estimated from known physiology, since there is approximately 70 ml of whole blood per kilogram of lean body weight in humans (47). Both  $A_1$  and  $A_2$  are set to the same value and equated to the ratio of the injected dose to the blood volume. Calculation of  $A_3$  is based on the known activity present in the blood at approximately 55 min. At this time, the first two exponential terms describing the blood time-activity curve have become negligible and a monoexponential function in terms of  $A_3$  and  $b_3$  is sufficient to describe the curve. Therefore, since we know  $b_3$ , back calculation to the zero time point of the sampled  $^{18}\text{F}$ FDG blood time-activity allows  $A_3$  to be estimated. From these data, the area under the blood curve may be estimated by using the previously described tri-exponential function.

## RESULTS

Tables 1 and 2 summarize the values for: MRDGlc determined by full kinetic analysis, DUR and MRDGlc determined by the SKM. The coefficient of determination ( $R^2$ ) for fitting the tissue time-activity data to the compartmental model was 0.98 pre-treatment and 0.99 post-treatment. Table 1 details the

**TABLE 2**  
Patients' Weight, Blood Glucose, DUR and True and SKM-MRDGlc

	Patient no.	Weight (kg)	Blood glucose ( $\mu\text{mole}/\text{min}/\text{g}$ )	True MRDGlc ( $\mu\text{mole}/\text{min}/\text{g}$ )	SKM-MRDGlc ( $\mu\text{mole}/\text{min}/\text{g}$ )	DUR
Pre-treatment	1	85	104	0.3309	0.2961	14.50
	2	54	61	0.2322	0.2319	14.55
	3	98	91	0.2590	0.2508	13.53
	4	68	74	0.1396	0.1666	8.93
	5	73	104	0.1796	0.1964	13.66
	6	65	74	0.1359	0.1487	11.14
	7	70	81	0.2073	0.2074	13.04
	8	58	68	0.3692	0.3527	17.44
	9	77	87	0.0871	0.1040	6.28
	10	75	90	0.1771	0.1790	6.84
	11	63	105	0.1968	0.2074	8.58
	12	56	134	0.2110	0.1926	6.32
	13	91	77	0.1796	0.2085	11.67
Post-treatment	1	85	79	0.0787	0.0999	6.90
	2	56	84	0.0624	0.0758	3.94
	3	94	92	0.0821	0.0947	5.43
	4	66	77	0.1005	0.1189	5.20
	5	69	109	0.0727	0.0986	4.76
	6	63	98	0.1113	0.1221	6.06
	7	69	100	0.1253	0.1391	7.48
	8	54	68	0.0443	0.0676	3.97
	9	77	76	0.0465	0.0580	3.62
	10	72	92	0.0873	0.0980	4.04
	11	63	96	0.0375	0.0495	2.04
	12	56	134	0.0416	0.0682	2.32
	13	91	86	0.0665	0.0973	4.96

The MRDGlc calculated from the full dynamic study is shown, together with the SKM value obtained by allowing for glucose metabolism in the whole body.

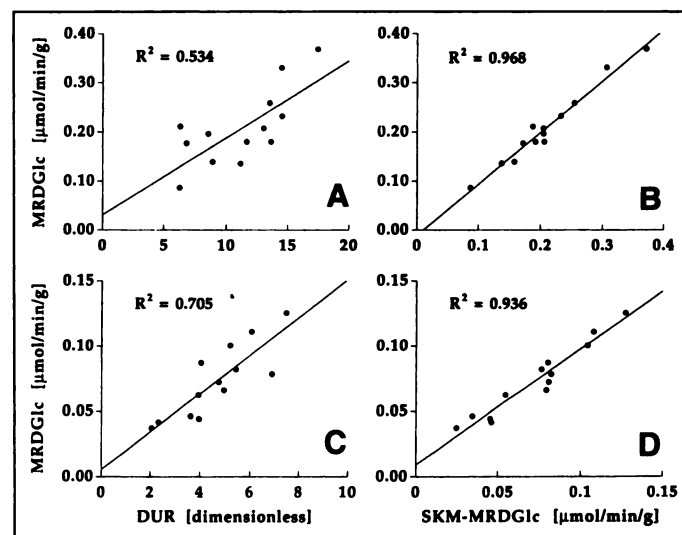
blood activity fitting parameters, as well as the means and standard errors (s.e.m.) for  $b_1$ ,  $b_2$  and  $b_3$ ;  $9.37 \pm .92$ ,  $0.29 \pm .02$  and  $0.0125 \pm 0.0007$  per minute, respectively. These values translate into decay half-times of 4.4 sec, 2.4 min and 55.5 min. It may be appreciated that in this group of patients, these decay constants are well defined and occupy narrow ranges.

Figure 1 shows scatter plots of the pre- and post-treatment correlations between MRDGlc and DUR, and MRDGlc and SKM. For the pre-treatment data, the  $R^2$  values are 0.53 and 0.97, respectively. The improvement in  $R^2$  was highly significant ( $p < 0.0001$ ). The post-treatment  $R^2$  values were 0.71 and 0.94, respectively. Again the incremental improvement was very significant ( $p < 0.0004$ ). Figure 2A shows the regression between pooled pre- and post-treatment MRDGlc and DUR,  $R^2 = 0.81$ . Figure 2B shows the regression between pooled pre- and post-treatment MRDGlc and MRDGlc predicted by the SKM;  $R^2 = 0.98$ . It should be noted that data in Figures 1 and 2 includes the effects of the systematic bias caused by the omission of the  $\alpha$  term in Equation 5. The regression line was  $\text{MRDGlc} = 1.14 \times (\text{estimated MRDGlc}) - 0.0032$ . Figure 3 shows the correlation between the true area under the whole blood time-activity curve up to 55 min and the estimated area obtained by using mean values for the decay constants,  $R^2 = 0.98$ .

## DISCUSSION

Currently, DUR as an index of glucose metabolism in neoplasia is in widespread use for the classification of lesions into benign or malignant categories and for monitoring their response to treatment (48-53). Some of these studies, however, have reported inconsistent cutoff values for DUR in separating

malignant from benign tissue (37,50,51), while others have failed to reach a consensus on this matter (48,49,51). The present study arose from the need to reconcile the poor correlation ( $R^2 = 0.53$ ) of DUR with MRDGlc that we observed in our data, obtained for the clinical evaluation of



**FIGURE 1.** Scatter diagrams of DUR (A, C) and SKM values for MRDGlc (B, D) versus true MRDGlc calculated before (A, B) and after (C, D) treatment. (A) DUR versus true MRDGlc before treatment,  $R^2 = 0.53$  ( $p < 0.005$ ). (B) SKM-MRDGlc versus true MRDGlc before treatment,  $R^2 = 0.97$  ( $p < 0.0001$ ). (C) DUR versus true MRDGlc after treatment,  $R^2 = 0.71$  ( $p < 0.0003$ ). (D) SKM-MRDGlc versus true MRDGlc after treatment.  $R^2 = 0.94$  ( $p < 0.0001$ ).

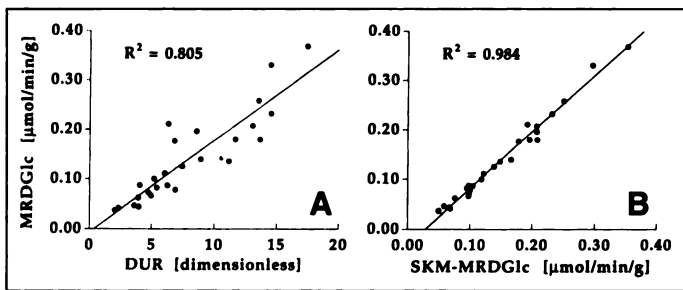


**FIGURE 2.** Scatter diagrams of DUR (A) and SKM-MRDGlC (B) versus true MRDGlC in all patients before and after treatment. The coefficients of determination,  $R^2 = 0.81$  ( $p < 0.001$ ) and  $R^2 = 0.98$  ( $p < 0.0001$ ) are somewhat improved compared with the individual pre- and post-treatment values. This is explained by the tighter grouping of the low values in the post-treatment group which tends to reduce overall scatter.

advanced lung cancer. This led us to examine the calculation of DUR and how it relates to the compartmental analysis used in the quantification of glucose metabolic rates in both normal and abnormal tissues.

Inherent in obtaining the dose uptake ratio in tumor tissue, consideration of the effects of whole body glucose metabolism has been omitted; that is, only tumor  $^{18}\text{F}$ FDG activity is used in the calculation of the DUR. However, the tissue activity recorded in a static study actually depends on the *history* of whole body metabolism, as well as the MRDGlC of the tissue under investigation. This history is reflected in the shape and magnitude of the blood time-activity curve. The dependency of MRDGlC on this curve leads directly to the nonlinear relationship between DUR and tissue MRDGlC (see Eqs. 1–7) and may explain some of the inconsistencies reported in the literature (48,49,51).

Using the simplified kinetic method (SKM) described above, we were able to achieve a very significant improvement ( $p < 0.0001$ ) in predicting true tumor MRDGlC from a simple static acquisition. This requires only a single timed venous blood sample collected midway through the static acquisition, approximately 55 min after injection of  $^{18}\text{F}$ FDG. Neither the time of imaging nor the time of blood sampling is critical in this method. However, it is critical that these times are recorded and taken into account in the mathematical treatment of the data.

This method does contain a small systematic bias resulting from omission of the complex term represented by  $\alpha$  in Equation 5 and the simplistic constraint of  $A_1 = A_2$ . Other constraints could be used, for example, the ratio  $A_1/A_2$  determined from a population study with the full dynamic method. These biases lead to a deviation of the regression line from the line of identity, and compound the systematic error introduced by lack of knowledge of the lumped constant in tumor tissue. Nevertheless, these systematic errors do not reduce the value of the methodology we describe. Further random errors are introduced by individual variability in whole body glucose metabolism and the assumptions made concerning the coefficients  $A_1$ ,  $A_2$  and  $A_3$  in the tri-exponential description of the blood

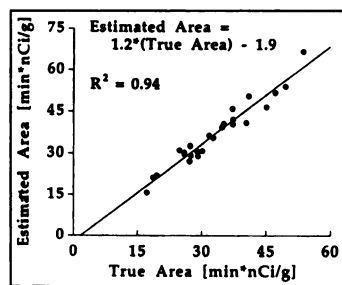


**FIGURE 3.** Scatter diagram of the estimated versus true area under the whole blood time-activity curve up to 55 min after injection. The coefficient of determination is high,  $R^2 = 0.94$ , and suggests that the method of area estimation is excellent.

time-activity curve. Figure 3 shows the relationship between the actual area under the whole blood time-activity curve and the calculated area; the coefficient of determination,  $R^2$ , was 0.94, which supports the notion that the method used for the estimation is valid. The random errors lead to scatter about the line of regression and are small since  $R^2 = 0.98$  in the pooled data set ( $n = 26$ ). Some of the systematic errors can be taken into account by adjusting for the slope and intercept of the regression line; this brings the linear relationship between the SKM values for MRDGlC and true MRDGlC to within the 95% confidence limits of the line of identity for the data ( $p > 0.5$ ). The effects of the lumped constant remain unknown but are assumed to be linear. Even though the metabolic behavior of the lung tumors that were studied is quite extreme, the correlation between SKM values for MRDGlC and the true values for MRDGlC was excellent. This suggests that application of this method in other, better metabolically behaved tumors should be straightforward.

## CONCLUSION

We believe that this methodology represents a substantial improvement over conventionally calculated DUR. It allows a quantitative prediction of MRDGlC to be made, while retaining the simplicity of a static,  $^{18}\text{F}$ FDG PET study for the assessment of advanced lung malignancy in patients. Its applicability in patients with less advanced lung cancer or other malignancies will require further study.

## ACKNOWLEDGMENTS

We thank Avis Loring and Steve Weise for their excellent technical assistance during this study and Dr. Elkan Halpern for invaluable statistical guidance.

## REFERENCES

- Sokoloff L, Reivich M, Kennedy C, et al. The [ $^{14}\text{C}$ ]deoxyglucose method for the measurement of local cerebral glucose utilization: theory, procedure and normal values in the conscious and anesthetized albino rat. *J Neurochem* 1977;28:897–916.
- Di Chiro G. Positron emission tomography using [ $^{18}\text{F}$ ] fluorodeoxyglucose in brain tumors: a powerful diagnostic and prognostic tool. *Invest Radiol* 1987;22:360–371.
- Nolop KB, Rhodes CG, Brudin LH, et al. Glucose utilization in vivo by human pulmonary neoplasms. *Cancer* 1987;60:2682–2689.
- Abe Y, Matsuzawa T, Fujiwara T, et al. Clinical assessment of therapeutic effects on cancer using 18F-2-fluoro-2-deoxy-D-glucose and positron emission tomography: preliminary study of lung cancer. *Int J Radiat Oncol Biol Phys* 1990;19:1005–1010.
- Ichihara Y, Kuwabara Y, Otsuka M, et al. Assessment of response to cancer therapy using fluorine-18-fluorodeoxyglucose and positron emission tomography. *J Nucl Med* 1991;32:1655–1660.
- Gupta NC, Frank AR, Dewan NA, et al. Solitary pulmonary nodules: detection of malignancy with PET with 2-[ $^{18}\text{F}$ ]fluoro-2-deoxy-D-glucose. *Radiology* 1992;184:441–444.
- Minn H, Joensuu H, Ahonen A, Klemi P. Fluorodeoxyglucose imaging: a method to assess the proliferative activity of human cancer in vivo. Comparison with DNA flow cytometry in head and neck tumors. *Cancer* 1988;61:1776–1781.
- Haberkorn U, Strauss LG, Reisser C, et al. Glucose uptake, perfusion and cell proliferation in head and neck tumors: relation of positron emission tomography to flow cytometry [see comments]. *J Nucl Med* 1991;32:1548–1555.
- Baillet JW, Abemayor E, Jabour BA, Hawkins RA, Ho C, Ward PH. Positron emission tomography: a new, precise imaging modality for detection of primary head and neck tumors and assessment of cervical adenopathy. *Laryngoscope* 1992;102:281–288.
- Chen BC, Hoh C, Choi Y. Evaluation of primary head and neck tumor with PET-FDG [Abstract]. *Clin Nucl Med* 1990;15:758.
- Paul R. Comparison of fluorine-18-2-fluorodeoxyglucose and gallium-67-citrate imaging for detection of lymphoma. *J Nucl Med* 1987;28:288–292.
- Okada J, Yoshikawa K, Imazeki K, et al. The use of FDG-PET in the detection and management of malignant lymphoma: correlation of uptake with prognosis. *J Nucl Med* 1991;32:686–691.
- Okada J, Yoshikawa K, Itami M, et al. Positron emission tomography using fluorine-18-fluorodeoxyglucose in malignant lymphoma: a comparison with proliferative activity. *J Nucl Med* 1992;33:325–329.
- Kubota Y, Yamada K, Yoshioka S, Yamada S, Ito M, Ido T. Differential diagnosis of idiopathic fibrosis from malignant lymphadenopathy with PET and  $^{18}\text{F}$ -fluorodeoxyglucose. *Clin Nucl Med* 1992;17:361–363.
- Kuwabara Y, Ichihara Y, Otsuka M, et al. High [ $^{18}\text{F}$ ]FDG uptake in primary cerebral lymphoma: a PET study. *J Comput Assist Tomogr* 1988;12:47–48.
- Kern KA, Brunetti A, Norton JA, et al. Metabolic imaging of human extremity musculoskeletal tumors by PET. *J Nucl Med* 1988;29:181–186.

17. Adler LP, Blair HF, Makley JT, et al. Noninvasive grading of musculoskeletal tumors using PET. *J Nucl Med* 1991;32:1508–1512.
18. Hoh C, Hawkins RA, Glaspy J. PET total body imaging in breast cancer with  $^{18}\text{F}$  ion and FDG [Abstract]. *Clin Nucl Med* 1990;15:763.
19. Wahl RL, Cody R, Hutchins G, Mudgett E. Positron-emission tomographic scanning of primary and metastatic breast carcinoma with the radiolabeled glucose analog 2-deoxy-2- $^{18}\text{F}$ fluoro-D-glucose [Letter]. *N Engl J Med* 1991;324:200.
20. Wahl RL, Cody RL, Hutchins GD, Mudgett EE. Primary and metastatic breast carcinoma: initial clinical evaluation with PET with the radiolabeled glucose analog 2- $^{18}\text{F}$ fluoro-2-deoxy-D-glucose. *Radiology* 1991;179:765–770.
21. Harney JV, Wahl RL, Liebert M, et al. Uptake of 2-deoxy, 2- $^{18}\text{F}$  fluoro-D-glucose in bladder cancer: animal localization and initial patient positron emission tomography. *J Urol* 1991;145:279–283.
22. Francavilla TL, Miletich RS, DeMichele D, et al. Positron emission tomography of pituitary macroadenomas: hormone production and effects of therapies. *Neurosurgery* 1991;28:826–833.
23. De Souza B, Brunetti A, Fulham MJ, et al. Pituitary microadenomas: a PET study. *Radiology* 1990;177:39–44.
24. Strauss LG, Clorius JH, Schlag P, et al. Recurrence of colorectal tumors: PET evaluation. *Radiology* 1989;170:329–332.
25. Yonekura Y, Benua RS, Brill AB, et al. Increased accumulation of 2-deoxy-2- $^{18}\text{F}$ fluoro-D-glucose in liver metastases from colon carcinoma. *J Nucl Med* 1982;23:1133–1137.
26. Okazumi S, Isono K, Enomoto K, et al. Evaluation of liver tumors using fluorine-18-fluorodeoxyglucose PET: characterization of tumor and assessment of effect of treatment. *J Nucl Med* 1992;33:333–339.
27. Joensuu H, Ahonen A. Imaging of metastases of thyroid carcinoma with fluorine-18-fluorodeoxyglucose. *J Nucl Med* 1987;28:910–914.
28. Francavilla TL, Miletich RS, Di CG, Patronas NJ, Rizzoli HV, Wright DC. Positron emission tomography in the detection of malignant degeneration of low-grade gliomas. *Neurosurgery* 1989;24:1–5.
29. Alavi JB, Alavi A, Chawluk J, et al. Positron emission tomography in patients with glioma: a predictor of prognosis. *Cancer* 1988;62:1074–1078.
30. Schlag P, Lehner B, Strauss LG, Georgi P, Herfarth C. Scar or recurrent rectal cancer. Positron emission tomography is more helpful for diagnosis than immunoscintigraphy. *Arch Surg* 1989;124:197–200.
31. Minn H, Paul R, Ahonen A. Evaluation of treatment response to radiotherapy in head and neck cancer with fluorine-18-fluorodeoxyglucose. *J Nucl Med* 1988;29:1521–1525.
32. Minn H, Paul R. Cancer treatment monitoring with fluorine-18 2-fluoro-2-deoxy-D-glucose and positron emission tomography: frustration or future [Editorial]. *Eur J Nucl Med* 1992;19:921–924.
33. Hawkins RA, Choi Y, Huang SC, Messa C, Hoh CK, Phelps ME. Quantitating tumor glucose metabolism with FDG and PET [Editorial]. *J Nucl Med* 1992;33:339–344.
34. Lammertsma AA, Brooks DJ, Frackowiak RS, et al. Measurement of glucose utilization with  $^{18}\text{F}$ 2-fluoro-2-deoxy-D-glucose: a comparison of different analytical methods. *J Cereb Blood Flow Metab* 1987;7:161–172.
35. Fischman AJ, Alpert NM. FDG-PET in oncology: there's more to it than looking at pictures [Editorial]. *J Nucl Med* 1993;34:6–11.
36. Graham MM, Lewellen TK. Positron emission tomography and its role in metabolic imaging. *Mayo Clin Proc* 1989;64:725–727.
37. Kim CK, Gupta NC, Chandramouli B, Alavi A. Standardized uptake values of FDG: body surface area correction is preferable to body weight correction [see comments]. *J Nucl Med* 1994;35:164–167.
38. Langen KJ, Braun U, Kops RE, et al. The influence of plasma glucose levels on fluorine-18-fluorodeoxyglucose uptake in bronchial carcinomas. *J Nucl Med* 1993;34:355–359.
39. Lindholm P, Minn H, Leskinen-Kallio S, Bergman J, Ruotsalainen U, Joensuu H. Influence of the blood glucose concentration on FDG uptake in cancer—a PET study. *J Nucl Med* 1993;34:1–6.
40. Hamberg LM, Hunter GJ, Alpert NM, Choi NC, Babich JW, Fischman AJ. The dose uptake ratio as an index of glucose metabolism: useful parameter or oversimplification? *J Nucl Med* 1994;35:1308–1312.
41. Kilbourn MR, Hood JT, Welch MJ. A simple  $^{18}\text{O}$ -water target for  $^{18}\text{F}$  production. *Int J Appl Radiat Isot* 1984;35:599–602.
42. Hamacher K. Phase-transfer catalyzed synthesis of 4-S- $\beta$  D-glucopyranosyl-2-thio-D-glucopyranose (thiocellobiose) and 2-S- $\beta$  D-glucopyranosyl-2-thio-D-glucopyranose (thiosophorose). *Carbohydr Res* 1984;27:291–295.
43. Hamacher K, Coenen HH, Stocklin G. Efficient stereospecific synthesis of no-carrier-added 2- $^{18}\text{F}$ fluoro-2-deoxy-D-glucose using aminopolyether supported nucleophilic substitution. *J Nucl Med* 1986;27:235–238.
44. Rota KE, Herzog H, Schmid A, Holte S, Feinendegen LE. Performance characteristics of an eight-ring whole body PET scanner. *J Comput Assist Tomogr* 1990;14:437–445.
45. Phelps ME, Huang SC, Hoffman EJ, Selin C, Sokoloff L, Kuhl DE. Tomographic measurement of local cerebral glucose metabolic rate in humans with  $^{18}\text{F}$ 2-fluoro-2-deoxy-D-glucose: validation of method. *Ann Neurol* 1979;6:371–388.
46. Rhodes CG, Wise RJ, Gibbs JM, et al. In vivo disturbance of the oxidative metabolism of glucose in human cerebral gliomas. *Ann Neurol* 1983;14:614–626.
47. Guyton AC. Chapter 25. The body fluid compartments: extracellular and intracellular fluids; interstitial fluid and edema. In: *Textbook of medical physiology*, 8th ed. Philadelphia: W.B. Saunders; 1991:273–285.
48. Keyes JW, Harkness BA, Greven KM, Williams DW, Watson NE, McGuirt F. Pretherapy evaluation with PET of salivary tumors [Abstract]. *Radiology* 1993;147(suppl):189P.
49. Inoue T, Kim EE, Komaki R, et al. Detecting recurrent or residual lung cancer with FDG-PET. *J Nucl Med* 1995;36:788–793.
50. Lowe VJ, DeLong DM, Hoffman JM, Coleman RE. Optimum scanning protocol for FDG-PET evaluation of pulmonary malignancy. *J Nucl Med* 1995;36:883–887.
51. Gupta NC, Chandramouli B, Frank A, Dewan N, Scott W. PET FDG imaging for estimating probability of malignancy in solitary pulmonary nodules [Abstract]. *Radiology* 1993;147(suppl):189P.
52. Gupta N, Dewan N, Frank A, Mailliard J, Scott W. Presurgical evaluation of patients with suspected malignant pulmonary nodules using PET-FDG imaging [Abstract]. *J Nucl Med* 1993;34(suppl):20P.
53. Haberkorn U, Strauss LG, Dimitrakopoulou A, et al. Fluorodeoxyglucose imaging of advanced head and neck cancer after chemotherapy. *J Nucl Med* 1993;34:12–17.

# Thallium-201 Uptake, Histopathological Differentiation and Na-K ATPase in Lung Adenocarcinoma

Hironori Takekawa, Kazuo Itoh, Shosaku Abe, Shigeaki Ogura, Hiroshi Isobe, Masayori Furudate and Yoshikazu Kawakami  
*First Department of Medicine and Department of Nuclear Medicine, School of Medicine, Hokkaido University; and Third Department of Medicine, School of Medicine, Sapporo Medical University, Sapporo, Japan*

To clarify differences in accumulation in  $^{201}\text{Tl}$  scintigraphy, we examined the relationship between uptake of  $^{201}\text{Tl}$ , histopathological differentiation and Na-K ATPase. **Methods:** Thallium-201 SPECT was performed twice: 15 min (early scan) and 120 min (delayed scan) after intravenous injection of 3 mCi  $^{201}\text{Tl}$ -chloride. The uptake ratio of  $^{201}\text{Tl}$  was calculated and compared with the grade of differentiation and the staining pattern of Na-K ATPase. **Results:** The sensitivity of  $^{201}\text{Tl}$  SPECT for well-differentiated adenocarcinomas was lower than that for moderately and poorly

differentiated ones. The uptake ratio on the delayed scan was significantly lower in the well-differentiated group than that in the moderately and poorly differentiated groups. This parameter was also significantly higher in the Na-K ATPase-positive group than the -negative group. **Conclusions:** These results indicate that the uptake ratio of  $^{201}\text{Tl}$  SPECT may be a noninvasive indicator of the grade of pathological differentiation of adenocarcinoma and provide insight into the relationship among  $^{201}\text{Tl}$  SPECT, malignancy and Na-K ATPase.

**Key Words:** thallium-201 single-photon emission computed tomography; grade of differentiation; Na-K ATPase; adenocarcinoma of the lung

**J Nucl Med 1996; 37:955–958**

Received Apr. 17, 1995; revision accepted Sept. 7, 1995.  
 For correspondence or reprints contact: Hironori Takekawa, MD, Department of Respiratory Medicine, Nikko Memorial Hospital, 1-5-13 Shintomi-cho, Muroran 051, Japan.